J Solid State Electrochem (1999) 3: 121–134

REVIEW

R. Alcántara · P. Lavela · J.L. Tirado
E. Zhecheva · R. Stoyanova

Recent advances in the study of layered lithium transition metal oxides and their application as intercalation electrodes

Received: 15 May 1998 / Accepted: 24 July 1998

Abstract A review is presented on the extensive work carried out during the last 30 years on layered oxides structurally related to $LiCoO_2$ and $LiNiO_2$. The studies considered here range from the structural and chemical characterization of the layered solids to the detailed evaluation of their aptitude towards lithium deintercalation-intercalation reactions, which form the basis of their successful application in rechargeable battery technology. The different challenges remaining in this area, such as the development of advanced preparation procedures and the optimization of the electrochemical performance by controlled changes in composition, structure, and particle morphology, are discussed.

Key words Lithium transition metal oxides · Lithium batteries · Layered oxides · Intercalation reactions

Introduction

The demands for advanced energy storage systems have stimulated extensive research directed toward the replacement of lead and cadmium by other metallic elements which are environmentally less aggressive and provide high-energy-density batteries. The advantages of using the lightest metal, lithium, as the negative electrode was demonstrated earlier by the low weights and high cell voltages obtained. Moreover, the search for rechargeable lithium anode cells was facilitated by the reversible insertion of lithium found in many intercalation host lattices, which makes these solids suitable as active cathode materials. In this way, lithium intercalation compounds and reactions have attracted the interest of many researchers since the early 1970s. As a result of this extensive research, several commercial products emerged in the field of both primary and rechargeable systems. The initial success of the rechargeable products was soon overshadowed by problems associated with the poor reconstruction of the topography of metal surfaces on cycling. The metal ions deposited on the surface of the metal electrode during cell charge are at sites different to those from which they are released during cell discharge. Subsequently, the growth of lithium dendrites may take place on prolonged cycling, which results in poor cycleability and possible internal short-circuits. This problem has also limited the applicability of other less electropositive metals – such as zinc – in rechargeable systems. However, the problem with lithium is probably more dramatic as a consequence of the exothermic reaction with hydrogen release that may have explosive results. More recently, a substantial improvement in the performance of lithium rechargeable batteries was achieved by the application of the ''lithium-ion'' concept, which can be considered as a modification of a ''rocking-chair'' system, such as those previously reported in the literature [1–3]. In these batteries, both active electrode materials intercalate lithium reversibly and the back-and-forth motion of lithium ions from one intercalation host to the other takes place during cell charge and discharge.

For the negative electrode, much work has been carried out in order to obtain high-performance intercalation materials with low potential, as referred to the lithium electrode. Many forms of natural and artificial carbon with controlled texture, composition, and crystallinity have been examined for these purposes, and are used in the pioneering lithium-ion systems. More recently, new materials such as glassy tin oxides [4] and metal alloys [5] are alternative and promising options.

Concerning the cathode material in lithium-ion batteries, success is restricted until now to lithium interca-

R. Alcántara · P. Lavela · J.L. Tirado (✉)
Laboratorio de Química Inorgánica, Facultad de Ciencias, Universidad de Córdoba, Avda. San Alberto Magno s/n, E-14004 Córdoba, Spain

E. Zhecheva · R. Stoyanova
Institute of General and Inorganic Chemistry, Bulgarian Academy of Sciences, BG-1113 Sofia, Bulgaria

lation compounds of one of the following two groups of solids: the layered compounds $Li_{1-x}MO_2$ (M = Co, Ni) and the three-dimensional spinel structure compound $Li_{1+x}Mn_2O_4$ [1, 5–7]. The advantage of these solids arises from the easy preparation of the oxide cathodes, which can be manipulated and combined directly with the anode material in a discharged state with low risk. Using this advantage, Sony introduced in 1990 the first commercial lithium rechargeable battery, in which the active electrode materials are layered $LiCoO_2$ and graphite [8]:

$$LiCoO_2(\text{cathode}) + \square C_6(\text{anode}) \underset{\text{discharge}}{\overset{\text{charge}}{\rightleftharpoons}} Li_{1-x}CoO_2(\text{cathode}) + Li_xC_6(\text{anode}) \quad (1)$$

In the last decade, extensive research has been devoted to the performance of lithium rechargeable batteries. It was established that the main operating problem arises from the thermal instability and capacity drop, which result from irreversible structural and morphological changes in the electrode materials during consecutive charge-discharge cycles. To solve this problem, efforts are mainly focused on the solid state chemistry and electrochemistry of lithium transition metal oxides, i.e. to modify the electrochemical properties by variations in composition, cation distribution, crystallinity, texture, etc., that can be achieved by controlling the synthesis conditions or by different pre–treatments of these "standard" compounds, as described below.

Structure and electrochemistry of $LiNiO_2$ and $LiCoO_2$

$Li_{1-x}Ni_{1+x}O_2$

The crystal structure of $LiNiO_2$ was first described by Dyer et al. [9] as belonging to the cesium dichloroiodide, $CsCl_2I$, type. The crystals were found to be rhombohedral, space group $D_{3d}^5 - R\bar{3}m$. By using hexagonal axes, the unit cell parameters $a = 2.878$ Å and $c = 14.19$ Å were reported and the atoms were distributed in the following sets of equivalent positions: nickel atoms in 3a sites (0, 0, 0), lithium in 3b (0, 0, 1/2), and oxygen in 6c (0, 0, z)(0, 0, $-z$) with $z = 0.25$ (Fig. 1). The structure can also be regarded as a cubic close packing of oxygen ions, in which the (111) planes of octahedral interstices are filled in an ordered sequence by alternating layers of Ni and Li atoms, i.e., similar to α-$NaFeO_2$. The resulting value of $c/a = 4.93$ is slightly higher than the value expected for a perfect cubic close packing arrangement ($c/a = 2\sqrt{6} = 4.90$). The difficulties in the preparation of stoichiometric $LiNiO_2$ were reported a few years later by Goodenough et al. [10]. In that study, two different composition regions were found in the $Li_xNi_{2-x}O_2$ solid solutions. For $x < 0.6$, the disordered rock-salt type, $Fm\bar{3}m$, structure prevails, while the lithium content in the $0.6 \le x \le 1.0$ range allowed the formation of the layered $R\bar{3}m$ structure of α-$NaFeO_2$. A third region was examined by Bronger et al. [11], who found a monoclinic structure for $x > 1.3$. Later, the cation distribution of the non-stoichiometric solid $Li_{1-x}Ni_{1+x}O_2$ was further studied by Rietveld analysis of X-ray diffraction data [12]. It was found that the occupancy of 3a and 3b sites by Ni and Li atoms approached as x increased, leading to a statistical distribution for $x \ge 0.4$. In a detailed study of the catalytic properties of the $Li_{0.45}Ni^{2+}_{0.10}Ni^{3+}_{0.45}O$ oxide by Pickering et al. [13], the usefulness of the Rietveld refinement to assess the cation distribution in these solids was emphasized. Two models are used to describe the cation distribution in $Li_{1-x}Ni_{1+x}O_2$ [10, 12, 14, 15]. According to one of the models, the nickel in excess of the stoichiometric amount occupies the free sites in the LiO_2 layers, to give $[Li_{1-x}Ni_x][Ni]O_2$ [14, 15], whereas according to the other model a partial mixing of lithium and nickel in the "alien" layers (Li in NiO_2 and Ni in LiO_2 layers, respectively) occurs, giving $[Li_{1-x-\delta}Ni_{x+\delta}][Ni_{1-\delta}Li_\delta]O_2$ [12, 14, 15]. In the case of almost stoichiometric $Li_{1-x}Ni_{1+x}O_2$, the first model is considered to be more reliable [16]. Nevertheless, some cation mixing (δ is about 5%) has been reported for oxides with $x = 0.04$ [15]. Owing to the small scattering factor of Li, the X-ray diffraction (XRD) method does not enable us to specify the reactions of intrinsic disorder in nearly stoichiometric $Li_{1-x}Ni_{1+x}O_2$. In this respect, electron paramagnetic resonance (EPR) of Ni^{3+} can be used as a valuable tool for studying the reactions of intrinsic disorder in $Li_{1-x}Ni_{1+x}O_2$ [17].

On the other hand, the X-ray absorption spectroscopy techniques have been used as a powerful tool to obtain detailed information about the electronic structure and local environment of nickel atoms in the

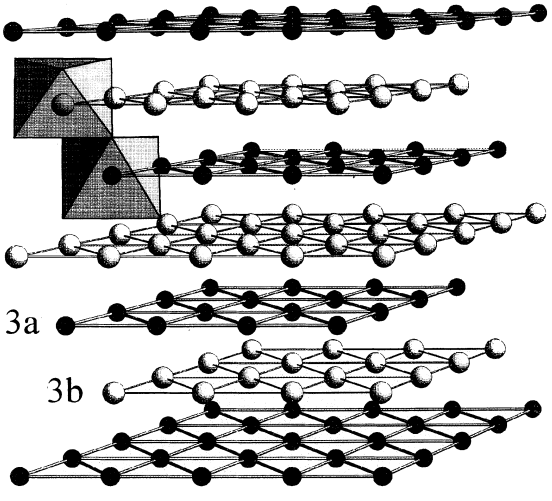

Fig. 1 Schematic representation of the layered structure of $LiMO_2$. Only 3a transition metal atoms (*black spheres*) and 3b lithium ions (*white spheres*) are fully displayed. One LiO_6 and one MO_6 representative octahedra are also included

structure of lithium nickel oxides. Pickering et al. [18] studied $Li_xNi_{1-x}O$ ($0 \le x \le 0.4$) compounds using Ni *K*-edge X-ray absorption fine structure (XAFS) spectroscopy. Extended XAFS (EXAFS) data showed two different Ni-O bond lengths (2.07 Å and 1.94 Å) with proportions varying with x. The systematic trends in X-ray absorption near-edge structure (XANES) data were interpreted in terms of a model in which the holes introduced by lithium ions reside predominantly on nickel atoms, consistent with an increasing nickel oxidation state with x rather than an increasing oxygen oxidation state from O^{2-} to O^{-}. Irrespective of the fact that lithium nickel oxides are considered as model systems in solid state physics, the electronic structure of these systems is still in controversial discussion [19]. EPR measurements of $LiNiO_2$ give direct evidence for the appearance of low-spin Ni^{3+} ions [20, 21], while the data on high-energy electron spectroscopy can be interpreted in terms of holes in the O 2*p* band [22, 23]. The ionic model of localized electron states with a 3*d* character is consistent with electric and magnetic measurements [10, 24–26], but cannot explain the absence of cooperative Jahn-Teller distortion in $LiNiO_2$. Chadwick et al. [27, 28] studied the cooperative Jahn-Teller distortion of Ni^{3+} ions in $LiNiO_2$ by EXAFS. It has been found that the local NiO_6 octahedron is distorted, possessing two long (2.09 Å) and four short (1.91 Å) Ni-O distances. Since the oxy-redox properties of $Li_{1-x}Ni_{1+x}O_2$ are comprehensible in the framework of Ni^{3+}/Ni^{4+} couples, it is widely accepted to use the ionic model with localized Ni^{3+} states for explanation of the electrochemical properties of lithium nickel oxide systems [1–3, 6, 7].

Lithium has been extracted (deintercalated) from $LiNiO_2$ by both chemical and electrochemical procedures. The electrochemical behavior of $LiNiO_2$ electrodes has been examined in detail by different authors by differential chronopotentiometry [29, 30] and cyclic voltammetry techniques [16, 31–36]. Thus, it is known that $LiNiO_2$ can be oxidized to $Li_{0.06}NiO_2$ without the destruction of its core structure [29]. The retention of the layered character of the structure is assumed to be achieved by partial migration of nickel ions from the NiO_2 layers to the depleted LiO_2 layers. After initial interpretations based on a single-phase process, it is now firmly established that lithium extraction from $LiNiO_2$ takes place through three coexisting-phase regions [29, 30, 34] (Fig. 2). These regions are the result of three first-order transformations: hexagonal to monoclinic, monoclinic to hexagonal, and hexagonal to hexagonal [29]. The structural relationships between the hexagonal and monoclinic ($C2/m$, similar to $NaNiO_2$) phases is given by: $a_m = \sqrt{3}a_h$, $b_m = a_h$, $c_m = c_h/(3 \sin \beta)$, $\beta = 180 - \tan^{-1}(c_h/\sqrt{3}a_h)$.

In addition, the non-stoichiometry of $Li_{1-x}Ni_{1+x}O_2$ was shown to have a direct effect on the charge profile and reversibility of the intercalation reaction [16, 34] as the impurity Ni^{2+} ions are known to deteriorate the electrochemical properties of $Li_{1-x}Ni_{1+x}O_2$ (Fig. 3).

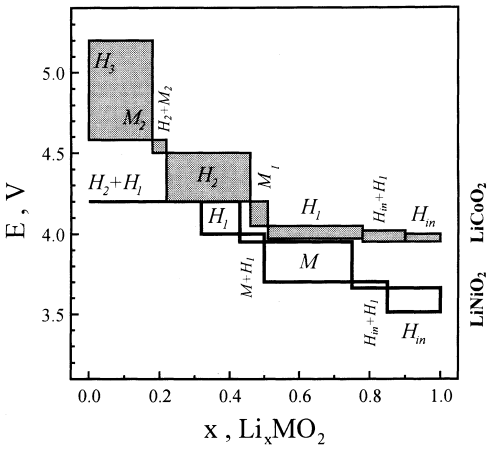

Fig. 2 Schematic representation of the structural changes during lithium extraction from $LiNiO_2$ and $LiCoO_2$. *H* and *M* denote the hexagonal and monoclinic structure, respectively

Arai et al. [34] observed four steep peaks in incremental capacity plots of a nearly stoichiometric sample ($x = 0.005$), prepared by using an excess of lithium, while larger x values did not allow their observation.

On the other hand, it was recently shown that the shape of the charge-discharge profile changes significantly with the recording rate [31]. While the first cycle of the voltammetry of $LiNiO_2$ electrodes recorded at 30 mV/h which was reported by Broussely et al. [31] showed a profile which is highly coincident with the differential chronopotentiograms in previous work [29, 30], the different current peaks were not resolved in the cyclic voltammograms recorded at 300 mV/h. Moreover, the cell capacity showed a marked decrease on increasing the scan rate (see Fig. 3). Thus, a discharge capacity of 210 mAh/g for the first cycle was found by using 10 mV/h, while ca. 60 mAh/g was the first cycle discharge value observed at 100 mV/h. However, the capacity retention was close to 100% even at the higher scan rate after the fourth cycle.

In addition, Broussely et al. [31] reported that the profile of the second cycle does not coincide with that observed during the first charge-discharge voltammogram for a scan rate of 300 mV/h. This result contrasts with the dx/dV plots reported by Li et al. [30], in which several consecutive 100 h rate cycles were shown to give similar profiles. At the same time, lithium nickelate displays a greater loss in capacity after the first charge-discharge cycle (see Fig. 3) compared with the consecutive cycles: about 40 mAh/g is lost after the first cycle [37, 38].

High temperature and low temperature $LiCoO_2$

Two years after the nickel analogue, the structure of $LiCoO_2$ was described by Johnston et al. [39]. The structure was reported to be equivalent to that of $LiNiO_2$ by replacing Ni atoms by Co. The hexagonal unit cell parameters were now $a = 2.8166$ Å, $c = 14.052$ Å,

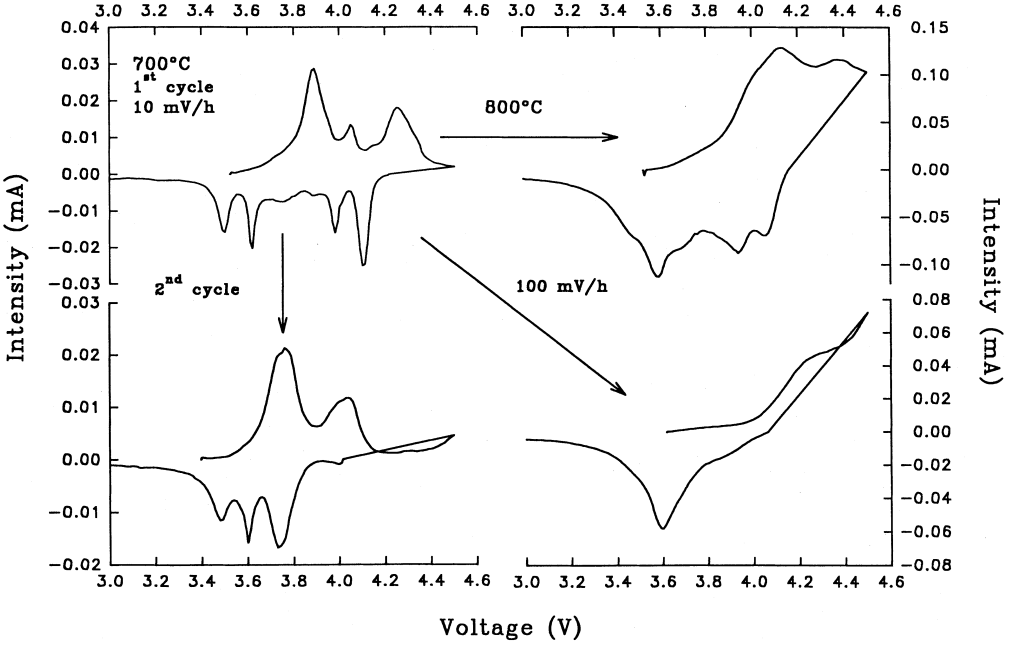

Fig. 3 Step potential electrochemical spectroscopy of lithium cells using a nearly stoichiometric $LiNiO_2$ sample obtained at 700 °C from citrate precursors. *Arrows* show the changes induced in the spectra *lower left corner* by recording the second cycle; *upper right corner* increasing the preparation temperature with a higher departure from the 1:1:2 stoichiometry; *lower right corner* increasing the scanning rate

$c/a = 4.989$, and the fractional coordinate of oxygen was $z = 0.26$ [40] (Fig. 1). The trigonal distortion of the cubic lattice for $LiCoO_2$ is higher than that of $LiNiO_2$, which is a result from the electronic structure of low-spin Co^{3+} (t_{2g}^6) and low-spin Ni^{3+} ($t_{2g}^6 e_g^1$) ions. In contrast to $LiNiO_2$, there is no doubt about the electronic structure of $LiCoO_2$: localized low-spin Co^{3+} states with a considerable covalent mixing account for the electronic structure of $LiCoO_2$ [41, 42]. When $LiCoO_2$ is synthesized at 400 °C, a structurally different powdered solid is formed [43–51]. This is referred to as the low-temperature (LT) modification in contrast to the rhombohedral high-temperature (HT) solid. About 6% of the cobalt ions are located in the lithium layers of the LT modification, as described from refinement of the powder neutron diffraction data [45]. The products of lithium extraction from this modification were also examined by X-ray and neutron diffraction [44]. A spinel-related model was proposed for Li_xCoO_2 ($1 \geq x \geq 0.5$), in which up to 80% of the remaining lithium could be located in tetrahedral sites [44]. Nevertheless, the refinement of the diffraction data of these solids in both a $R\bar{3}m$ layered structure and a $Fd\bar{3}m$ spinel-type structure was found to give comparable fits to the data [48].

LT-$LiCoO_2$ samples prepared at 400 °C were recently studied by $^{6,7}Li$ magic angle spinning (MAS) NMR [52]. Only a single peak at −1 ppm was observed, which showed a slightly broader signal compared to the materials obtained at higher temperatures. This was considered to be indicative of a larger structural disorder, but only in the second coordination sphere of lithium. Thus, all lithium ions were considered to be in octahedral sites and the structure of the LT oxide was described as an ordered cubic rock-salt structure instead of the description based on the spinel structure. In an attempt to obtain $Li_{1+y}CoO_2$, Carewska et al. [52] examined both ^6Li and ^7Li NMR spectra of the material obtained using excess lithium. The results showed that only a small fraction of the excess lithium enters interstitial sites of the structure in close proximity to the paramagnetic Co^{2+} ions.

The electrochemical lithium extraction-insertion process into HT-$LiCoO_2$ has been examined in detail by different authors, using high-precision voltage measurements as well as in situ XRD facilities [53–55]. The discharge curve of a HT sample prepared at 850 °C is shown in Fig. 4a. The main oxidation effect is observed for x values in the 0.75–0.95 range, leading to a current maximum in the I/V curve and a plateau in the V/x profile. These effects have been ascribed to the coexistence of a pristine $LiCoO_2$ phase with deintercalated solid, as a result of a first-order phase transition. A significant expansion of the hexagonal unit cell parameter c is observed in the deintercalated solid obtained for a low extent of cell charge. The expansion is due to increasing repulsion between the negatively charged CoO_2 layers as lithium is removed from the interlayer space. For higher voltages, two low-intensity current peaks occur at 4.05 V and 4.20 V, if the voltammogram is recorded at 25 °C. Reimers and Dahn [53] showed that the position of these peaks changes with the recording temperature. On increasing the temperature, both signals coalesce, while above 60 °C both are absent. These results have been interpreted in terms of an order-disorder phase transition involving the formation of a monoclinic ordered modification for the $Li_{0.5}CoO_2$

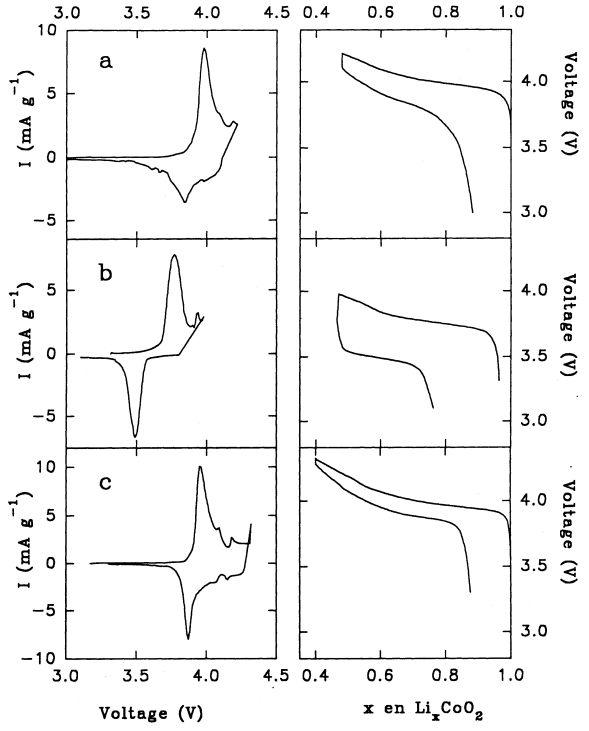

Fig. 4 *Left*: Normalized intensity versus voltage; *right*: voltage versus composition plots obtained by step potential electrochemical spectroscopy of lithium cells using different $LiCoO_2$ samples as the cathode: **a** high temperature (HT) $LiCoO_2$, **b** low temperature $LiCoO_2$, **c** boron-doped (5 at%) HT-$LiCoO_2$ sample

composition and further reconversion to the rhombohedral phase for higher potentials. The relationships between the hexagonal and monoclinic unit cell parameters are close to $a_m = \sqrt{3}a_h$, $b_m = a_h$, $c_m = c_h$, and $\beta = 90°$. The discharge characteristics of $Li_{0.4}CoO_2$ electrodes agree well with the good reversibility of the different phase transitions.

Until very recently, the stability of the deintercalated solid was thought to decrease monotonously for lithium extraction down to x values below 0.4. Mizushima et al. [56] explained the observed initial loss of stability as a result of the loss of binding lithium ions, while Reimers and Dahn [53] proposed an explanation of this phenomenon by assuming the destruction of the lattice on increasing the amount of the unstable Co^{4+} ions. Later, Ohzuku and Ueda [54] reported the formation of a monoclinic phase for $Li_{0.85}CoO_2$. Recently, Tarascon et al. [55] have claimed the preparation of the fully deintercalated solid. The hexagonal O1 modification ($a = 2.822$ Å, $c = 4.29$ Å) was obtained by avoiding liquid electrolytes in dry plastic lithium-ion cells. In this way, 95% of lithium could be reinserted in this solid. Recently, a direct correlation has been established between the large anisotropic changes in the structure and the electrochemical grinding for HT-$LiCoO_2$ occurring during electrochemical lithium extraction [57]. The changes in lattice dimensions during the extraction-insertion processes induce internal strains due to the mismatch between the zones with a different degree of intercalation in the solid [57]. These in turn lead to a highly stressed solid that develops cracks followed by particle fragmentation which destroy the crystallinity of the solid matrix and hence impair the cycleability of the cell [57]. In order to preserve good cycling performance for HT-$LiCoO_2$, the cycling of the practical cell proceeds over the composition range from $Li_{0.5}CoO_2$ to $LiCoO_2$ [58].

The kinetics of lithium intercalation into $LiCoO_2$ have been studied by different authors [38, 59, 60]. Both potentiostatic and galvanostatic intermittent titration procedures have been used as raw data in these studies. The divergences found in the values obtained using each approach are indicative of the difficulties of obtaining accurate data using methods which are usually developed for single-phase solid-solution systems, owing to the different phase transitions discussed above.

On the other hand, the electrochemical properties of LT-$LiCoO_2$ have also been investigated, irrespective of the lower potential and poorer reversibility found for this modification [45, 46, 48, 61, 62]. The intensity versus voltage curve (Fig. 4b) shows that the charge and discharge peaks are located at 3.77 V and 3.44 V for LT-$LiCoO_2$, respectively. These divergences from the HT modification were first reported by Gummow et al. [45, 46] and the corresponding plateaus were also detected by Rossen et al. [48]. However, some divergences in the interpretation of these effects can be found in the literature. Chronologically, the first hypothesis proposed was that the charge plateau corresponded to the coexistence of layered LT-$LiCoO_2$ and spinel $Li_{0.5}CoO_2$ [45]. An alternative interpretation was proposed [48] by ascribing the effect to the coexistence between spinel LT-$LiCoO_2$ and spinel $Li_{0.5}CoO_2$. A two-step extraction process of lithium from the octahedral sites was proposed during charge [46], while the insertion of lithium into tetrahedral and octahedral sites of a non-idealized spinel-type structure was assumed to take place at 3.7 V and 3.2 V, respectively, during cell discharge. Recently, Pereira-Ramos et al. [62] demonstrated from XRD data that a single-phase process describes accurately the charge process for LT-$LiCoO_2$ all along the lithium composition range $0.5 < x < 1$. Moreover, the limited expansion suffered by lithium extraction agrees well with the model proposed in which impurity Co^{3+} replace Li^+ ions and vice versa. This should avoid a large expansion such as that found in HT-$LiCoO_2$. Nevertheless, the larger difference between charge and discharge voltages of LT samples compared with HT samples may be indicative of a different reaction during discharge that could lead to the formation of different phases [62]. The differences found with HT electrodes were ascribed to the presence of ¼ Co atoms replacing Li atoms and vice versa, which interrupted the diffusion pathway for Li^+ ions, leading to lower chemical diffusion coefficients. Charged HT cathodes with $Li_{1-x}CoO_2$ compositions ($x = 0.1$, 0.4, and 0.6) were recently studied by lithium-7 NMR and EPR [63]. EPR signals due to spins localized

on the Co ions were observed. These spins resulted in dramatic chemical shifts and line broadening. To our knowledge, no spectroscopy data have been reported to assess the local structure of LT-$LiCoO_2$ electrodes and the changes induced by the deintercalation/intercalation process that could explain the differences in the electrochemical behavior of both modifications.

$Li_{1-x}(Ni_{1-y}Co_y)_{1+x}O_2$ solid solutions

Summarizing the electrochemical data on $LiCoO_2$ and $LiNiO_2$, it appears that $LiCoO_2$ is more suitable as a cathode material in a lithium-ion cell. Irrespective of the fact that $LiNiO_2$ is cheaper and exhibits a slightly higher reversible capacity than $LiCoO_2$, the dramatic sensitivity of the electrochemical properties of $LiNiO_2$ on the preparation procedure restricts its utilization. To optimize the electrochemical behavior of $LiCoO_2$ and $LiNiO_2$, $LiNi_{1-y}Co_yO_2$ solid solutions have been systematically investigated.

The preparation and characterization of homogeneous $LiNi_{1-y}Co_yO_2$ compounds ($0 \le y \le 1$) were first reported by Ohzuku et al. [64] and studied in detail by Delmas and Saadoune [65]. The rhombohedral $R\bar{3}m$ structure was observed in the complete composition interval. On increasing y, an almost linear decrease in the hexagonal unit cell dimensions was observed, while c/a increased. Up to 0.6 lithium could be deintercalated between 3.5 V and 4.0 V in lithium cells [64–67]. The stabilization of the layered crystal structure of $LiNiO_2$ by cobalt substitution was reported by Zhecheva and Stoyanova [68], who found that on increasing the y value in $Li_x(Ni_{1-y}Co_y)_{2-x}O_2$ solid solutions the nonstoichiometry parameter x reached values close to unity.

Further insight into the structure of the solid solutions was reported by Ohzuku et al. [69], who showed by magnetic susceptibility measurements that $LiNi_{1-y}Co_yO_2$ consists of low-spin states of $Co^{3+}(t_{2g}^6e_g^0)$ and $Ni^{3+}(t_{2g}^6e_g^1)$. A detailed electrochemical study on the rhombohedral phase with $LiNi_{1/2}Co_{1/2}O_2$ stoichiometry and $a_h = 2.84$ Å, $c_h = 14.1$ Å unit cell parameters was later reported by Ueda and Ohzuku [70]. The solid was obtained by reacting mixtures of the carbonates of the three elements in exact proportions at 900 °C. Lithium cells using this solid as the active cathode material showed a reversible oxidation at about 3.5 V, which was accompanied by an almost linear increase of the c unit cell parameter as a function of x in $Li_{1-x}Ni_{1/2}Co_{1/2}O_2$ up to ca. 0.5. Changes in the slope of the OCV (Open Circuit Voltage) curves at $x = 1/3$ and 1/4 were interpreted as a lithium ordering process.

The structure of $LiNi_{1-y}Co_yO_2$ was further examined by Delmas et al. [71, 72] by using ^6Li and ^7Li NMR. From these studies it was demonstrated that microheterogeneities at the length scale of the chemical bond were present in the lattice of $LiNi_{1-y}Co_yO_2$ solid solutions. A tendency to depart from a random Ni/Co distribution in the $Ni_{1-y}Co_yO_2$ layers by the formation of cobalt clusters was shown from the NMR spectra. Later, Ni^{3+} EPR measurements were used to investigate the electronic structure and ion distribution of $Li_{1-x}(Ni_y\,Co_{1-y})_{1+x}O_2$ ($y = 0.13$ and $0.8 \le y \le 1.0$) solid solutions obtained between 450 °C and 800 °C by Stoyanova et al. [73]. From the analysis of the EPR linewidth for $LiNi_{1-y}Co_yO_2$ solid solutions, information has been extracted on the Ni^{3+}/Co^{3+} short-range order in the $Ni_yCo_{1-y}O_2$ layers, which expands up to a distance of $2a$ [73]. Furthermore, changes in the intensity ratio of Ni^{3+} EPR signals with $g = 2.142$ and 2.137, which are assigned to isolated and non-isolated Ni^{3+} ions, respectively (Fig. 5), show that a transition from a non-random to a random Ni/Co distribution in the $Ni_yCo_{1-y}O_2$ slabs occurs between 650 °C and 750 °C. The changes in the intensity ratio obtained from the signals of the ^6Li MAS NMR spectra at 0 and −15 ppm (Fig. 5), assigned to the appearance of $\{Li(Co_3Co_3)^I(Co_3Co_3)^{II}\}$ and $\{Li(Co_3Co_3)^I(Ni_1Co_5)^{II}\}$ configurations, respectively, are in good agreement with this interpretation [73].

Saadoune and Delmas [74] have revised the conduction properties and electrochemical performance of $Li_{1-y}Ni_{1-y}Co_yO_2$ solid solutions. According to this report, pristine cobalt-rich compositions show a lower conductivity than Ni-rich compositions, but increase the conductivity on deintercalation by a direct Co-Co conduction process via the t_2-t_2 orbitals.

The effect of temperature and composition on the electrochemical behavior of $Li_{1-x}(Ni_yCo_{1-y})_{1+x}O_2$ ($y = 0.88$ and 0.13) solid solutions obtained in the 450–800 °C temperature range was recently studied by Alcántara et al. [75] using step potential electrochemical spectroscopy. It was shown that the intensity versus voltage curves for cobalt-rich compositions display two

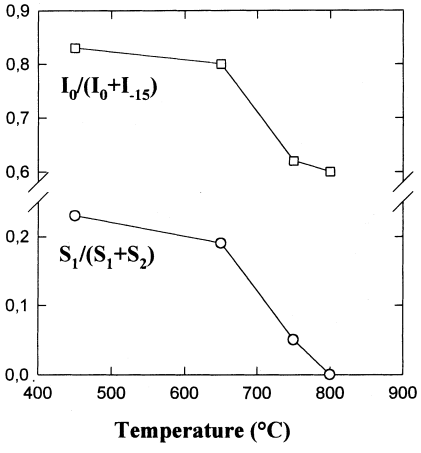

Fig. 5 Changes in the intensity ratio of ^6Li magic angle spinning nuclear magnetic resonance (MAS NMR) and Ni^{3+} electron paramagnetic resonance (EPR) signals in the spectra of $Li_{1-x}(Ni_{0.13}Co_{0.87})_{1+x}O_2$ obtained at different temperatures. *Upper*: $I_0/(I_0+I_{-15})$ ratio obtained from the signals of the ^6Li MAS NMR spectra at 0 and −15 ppm. *Lower*: $S_1/(S_1+S_2)$ ratio computed from the EPR line intensities of the signals with $g = 2.142$ (S_1) and $g = 2.137$ (S_2)

well-defined signals during cell charging, which are located at ca. 3.6 V and 3.9 V. The low-voltage signal is due to nickel oxidation. For samples prepared below 750 °C, the first step of the deintercalation from the pseudo-spinel phase contributes to this effect, while the second is responsible for the 3.9 V peak. For samples above 650 °C, the single-phase extraction preserves the trigonal lattice up to 4.2 V with a marked increase in the c/a ratio. For Ni-rich compositions, cell performance is poor for samples prepared below 750 °C. However, the sample prepared at 750 °C shows reversible extraction by a single-phase mechanism and a simple voltammogram, which differs markedly from the $LiNiO_2$ electrodes. Ex situ EPR of Ni^{3+} ions in the electrodes after the first cycle reveals a better recovery of the oxidation state of metal ions for the nickel-rich composition at 750 °C [75].

Advanced preparative procedures of $LiNiO_2$ and $LiCoO_2$

It is well known that the electrochemical performance of oxide materials is concurrently affected by three basic parameters: composition, structure, and morphology. These properties are affected by the preparation procedure used to obtain the powdered solids as active electrode materials. Thus, a great deal of effort has been devoted to the development of alternative chemical routes for the preparation of $LiCoO_2$ and $LiNiO_2$. Particularly, the soft-chemistry techniques for materials design enable the preparation of ultrafine materials with homogeneous composition and particle morphology, which are useful as high-rate electrodes that show good cycling behavior at high charge/discharge rates. This advantage makes the soft-chemistry methods very suitable for industrial scale-up.

To prepare both novel and previously known materials with controlled compositions, structure, and morphology, various low-temperature techniques have been developed [76–78]. Summarizing the literature data on the low-temperature preparation of $LiCoO_2$ and $LiNiO_2$, three variants of the soft-chemistry methods may be pointed out: (1) sol-gel processes; (2) metal-inorganic/organic precursors; and (3) ion-exchange reactions.

In basic media, layered $LiCoO_2$ has successfully been prepared by a sol-gel method using an aqueous solution of Li-Co acetates, followed by heat treatment at 500 °C [79]. This method allows preparation of $LiCoO_2$ as a bulk material or as thick films. Recently, Oh et al. [80] have elaborated a sol-gel method for the preparation of ultrafine $LiCoO_2$ and monodisperse $LiNiO_2$ [81], where poly(acrylic acid) and poly(vinylbutyral) serve as chelating agents. Layered $LiCoO_2$ powders can be obtained when the gel precursor is heated at 550 °C, while a temperature of 750 °C is required for the preparation of layered $LiNiO_2$.

Hydrolysis of Co^{III} coordination compounds with LiOH yields different phases in the Li-Co-O system [82]. The hydrolysis of $Co(NH_3)_6^{3+}$ gives mixtures of $LiCoO_2$ and $HCoO_2$ as ultrafine particles. A high $[OH^-]/[Li^+]$ ratio resulted in a higher $HCoO_2$ content. Attempts were also made to prepare lithiated phases by the hydrolysis of $Co(acac)_3$ suspensions, where acac is acetylacetonate. The product of this reaction yielded exclusively $Co(OH)_2$.

Spinel-related $LiCoO_2$ has been synthesized by a solution technique, according to which lithium and ammonium hydroxide react with an aqueous cobalt nitrate solution to form hydroxide-nitrate precursors [50]. The precursors thus prepared were heat treated at temperatures as low as 300 °C.

Taking into account the present low-temperature techniques for material design, it seems that the organic polyfunctional acids should have great potential in the preparation of ultrafine layered $LiCoO_2$ and $LiNiO_2$. The complexation between Co/Ni and the organic acids via functional groups allows researchers to obtain and modify the metal-organic precursors at a molecular level. Thermal heating of organic acid complexes (such as malic and succinic acids) of Li/Co at 900 °C in air yields well-crystallized, layered $LiCoO_2$ [83]. Recently, Yazami et al. [84] have elaborated a new synthetic method of high surface area $LiCoO_2$ powders, characterized by a layered crystal structure. This method consists of thermal decomposition of an intimate mixture of lithium acetate and cobalt acetate at 550 °C under air for at least 2 h. $LiCoO_2$ thus prepared shows higher performance in terms of cell capacity compared with the high-temperature analogues [84]. On increasing the intensity of the current passing through the cell, the decrease in cathode utilization is less marked for LT samples. Thus, LT electrodes show higher capacities than HT electrodes at high current intensities. This effect has been explained in terms of a quick electrode polarization in the HT electrode, owing to the increased lithium-ion concentration gradient, as a result of the lower active surface area.

Based on the precursor method, the synthesis of $LiCoO_2$ using electrostatic spray pyrolysis [85], chemical vapor deposition [85], physical vapor deposition [86–89], spray pyrolysis [86, 90–92], radiofrequency magnetron sputtering [92], and a spray-coating process [93], followed by some post-annealing to form the layered structure, have been reported for the production of thin film electrodes.

The citrate precursor method was successfully used in the preparation of finely dispersive layered $LiCoO_2$ and $LiNiO_2$ [17, 94–95]. This method consists of the thermal decomposition of Li-Co/Ni citrates. Citric acid acting as a chelating agent was used to mix Li and Co/Ni at an atomic scale in the precursors. Freeze drying [17, 95] or ethanol dehydration [94] of lithium-cobalt/nickel-organic acid solutions ($pH = 7$) yield homogeneous Li-Co/Ni citrate precursors, where Co^{2+} or Ni^{2+} ions are complexed by citric acid via hydroxy and carboxylate groups and Li^+ ions serve as counter ions.

Between 400 and 600 °C the thermal decomposition of freeze-dried or ethanol-dehydrated Li-Co citrate

precursors yields $LiCoO_2$ with a layered and pseudo-spinel structure through a complex exothermal effect (Fig. 6). The proportion between both modifications of $LiCoO_2$ is dependent on: (1) the Co/organic acid ratio; (2) the concentration of the freeze-dried solution; and (3) the heating rate [94, 95]. These products contain negligible amounts of residual carbon (about 0.02 wt%). With the metal citrate method, we did not succeed in preparing single-phase $LiCoO_2$ with a pseudo-spinel structure [95]. At 400 °C the most defectless layered $LiCoO_2$, consisting of hexagonal individual particles with dimensions of 80–120 nm, is a product of the bis-citrate $(NH_4)_3LiCo(C_6H_5O_7)_2$ decomposition at a slow heating rate [94, 95]. This product can be annealed up to 800 °C without marked structural changes. The $LiCoO_2$ powder was used as the active cathode material in lithium cells. Cyclic voltammograms showed little changes with synthesis temperature in the main cathodic and anodic peaks. For ultrafine layered $LiCoO_2$ and $LiCoO_2$ obtained by solid state reaction at high-temperatures (850 °C), the deintercalation and intercalation reactions proceed in the 3.95–3.99 and 3.86–3.88 voltage intervals, respectively. The loss of cell capacity is limited in electrodes prepared at 400 °C [94, 95].

A lithium nickel citrate, $LiNi(C_6H_5O_7) \cdot x\ H_2O$, is a very appropriate precursor for the preparation of nearly stoichiometric submicron $Li_{1-x}Ni_{1+x}O_2$ ($x \leq 0.05$) within the temperature range 700–800 °C [17]. Using EPR of low-spin Ni^{3+}, it was shown that the cation distribution in $Li_{1-x}Ni_{1+x}O_2$ depends on the synthesis temperature: the lower synthesis temperatures (700 °C) suppress the reactions of intrinsic disorder in the layers. The $LiNiO_2$ powder was used as the active cathode material in lithium cells. The cyclic voltammograms using the cathode material prepared by thermal decomposition of the non-crystalline products of freeze-dried citrate solutions showed several current peaks during the first cycle, resulting from the formation of the intermediate phases usually found in quasi-stoichiometric $LiNiO_2$. Such behavior is clearly ascribable to a highly stoichiometric material, irrespective of the fact that no lithium excess was required during the preparation. This gives additional interest to the metal/organic precursor method in the lithium-nickel oxide system to obtain almost stoichiometric $LiNiO_2$ with high electrochemical performance. After the almost complete extraction of lithium, further cycles reveal a significant loss of capacity and changes in the number of current peaks as a result of the changes induced in the structure of the solid. EPR data on cycled $LiNiO_2$ show partial migration of Ni from 3a (nickel layers) to 3b sites (lithium layers) [17].

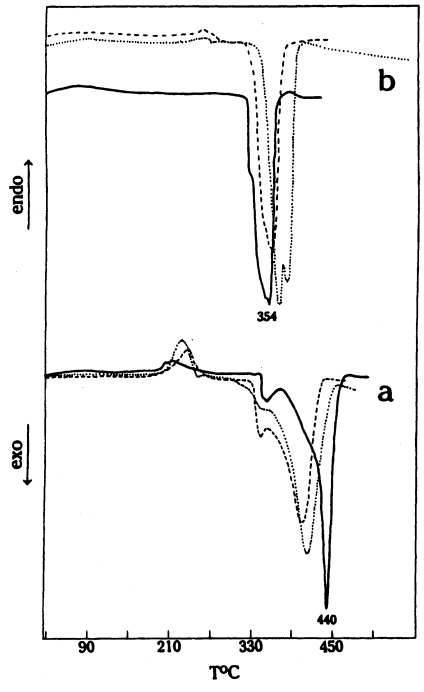

Fig. 6 Differential scanning calorimetry curves of lithium cobalt bis (citrate) (**a**) and lithium cobalt citrate (**b**), prepared by freeze drying of solutions with 0.05 M Co (*solid line*) and 0.5 M Co (*dotted line*). The *dashed line* corresponds to the ethanol dehydrated samples

The ion exchange reaction provides a new opportunity for the synthesis of active cathode materials [96–98]. The structural relationships between $LiCoO_2$ and $HCoO_2$ were recently used as an interesting tool in the low-temperature preparation of $LiCoO_2$ by Tarascon et al. [97]. A complete conversion to the $LiCoO_2$ phase was achieved by the ion exchange reaction between CoOOH and an excess of $LiOH \cdot H_2O$ carried out at 160 °C and an air pressure of 60 bar for 2 days. From coupled transmission electron microscopy and XRD studies, Tarascon et al. [97] concluded that the reaction occurs by surface H^+/Li^+ exchange and is accompanied by a progressive breaking of the particles owing to an interfacial collapse phenomenon. The $LiCoO_2$ powders obtained by this procedure were contaminated by carbonates. Heating these powders at moderate temperatures of ca. 250 °C was effective in removing the contaminant species and drastically improving their electrochemical cycling properties. The same ion exchange reaction was successfully applied to the synthesis of $LiNiO_2$ [98]. By controlling the ion-exchange parameters, layered $LiMO_2$ products can be prepared that exhibit electrochemical performance comparable to that of high-temperature phases.

Ion exchange and chemical deintercalation of $LiNiO_2$ and $LiCoO_2$

The effect of acid treatment on alkali metal-transition metal oxides may be classified as alkali ion extraction and proton exchange. Additional divergences in the chemical behavior of lithium cobaltate and nickelate result from their behavior in protonic acid media.

Chemical deintercalation in $LiNiO_2$

As early as 1954, Dyer et al. [9] observed that HCl treatment of $LiNiO_2$ resulted in a partial dissolution, accompanied by Cl_2 release. This process was studied by Morales et al. [12] in 1990, who showed that the room temperature treatment of $Li_{1-x}Ni_{1+x}O_2$ powders with aqueous HCl did not induce a Li^+/H^+ exchange process. Instead, a chemical deintercalation reaction takes place by which Ni^{3+} disproportionates, according to the following reaction:

$$(1-x+y)Li_{1-x}Ni_{1+x}O_2(s) + 4yH^+(aq) \rightarrow (1-x)Li_{1-x-y}Ni_{1+x}O_2(s) + y(1+x)Ni^{2+}(aq) + 2y(1-x)Li^+(aq) + 2yH_2O(\ell) \quad (2)$$

The partial dissolution of the oxide occurred simultaneously by a parallel reaction with Cl_2 release, according to:

$$2Li_{1-x}Ni_{1+x}O_2(s) + 2(1-x)Cl^-(aq) + 8H^+(aq) \rightarrow 2(1+x)Ni^{2+}(aq) + 2(1-x)Li^+(aq) + (1-x)Cl_2(g) + 4H_2O(\ell) \quad (3)$$

Cation distribution in the chemically deintercalated oxide samples was found to be similar to the distribution observed in electrochemically deintercalated $LiNiO_2$ [49, 99, 100]. Moreover, it was recently found that the monoclinic distortion resulting in $LiNiO_2$ charged electrodes is also present after chemical deintercalation [99]. The solid shows a $C2/m$ structure ($a \approx 4.95$ Å, $b \approx 2.82$ Å, $c \approx 5.04$ Å, $\beta \approx 109.2°$ [99]). In addition, the room-temperature single-line EPR spectra of nearly stoichiometric $LiNiO_2$ with $g = 2.137$ changes to $g = 2.195$ in the monoclinic form [99]. This effect is a consequence of the decreasing covalent character of the Ni-O bond on deintercalation. Also, the linear dependence of the EPR linewidth with the registration temperature is preserved on deintercalation, although the slope of the line decreases after extraction of up to 0.2 Li per mol. These changes are due to the structural modification of the solid as well as to the replacement of Ni^{3+} by diamagnetic low-spin Ni^{4+} ions. For non-stoichiometric $Li_{1-x}Ni_{1+x}O_2$, it has been found that the short-range and long-range cation orders specify their behavior toward acids, as was discussed above for the electrochemical performance [101]. For $Li_{1-x}Ni_{1+x}O_2$ with $0.6 < x < 0.9$, where a partial cation order occurs, acids remove lithium ions and statistically distributed impurity nickel ions from the LiO_2 layers, but do not attack Ni^{2+} and Ni^{3+}, which are segregated in the neighboring (111) cubic planes [101].

The thermal treatment of the acid-delithiated oxide results in an irreversible transformation at ca. 200 °C [12, 25, 102, 103]. The thermal transformation leads to a cubic spinel phase ($a \approx 8.08$ Å) with oxygen release. The process is also similar to that found in the electrochemically deintercalated solid and leads to a poor performance of the lithium anode cells using the thermally treated solid as the cathode material.

Proton exchange in $LiCoO_2$

Li^+/H^+ exchange was first studied by Fernández et al. [104]. The hydrothermal treatment of $LiCoO_2$ powders with HCl solutions at 200 °C and autogenic pressure yields the isostructural oxyhydroxide, according to the biphasic ion-exchange reaction:

$$LiCoO_2(s) + H^+(aq) \rightarrow HCoO_2(s) + Li^+(aq) \quad (4)$$

According to Delaplane and Ibers [105] and Fernández et al. [104, 106], the crystal structure of $HCoO_2$ belongs to the trigonal $R\bar{3}m$ space group with cobalt in 3a, hydrogen in 3b, and oxygen in 6c sites. A lower unit cell parameter c (13 Å) and a larger z_{oxygen} parameter (0.41) are found in cobalt oxyhydroxide compared with $LiCoO_2$.

At room temperature, acid acts toward layered $LiCoO_2$ not only as a delithiating agent but also as a hydrolyzing agent, as a result of which a metastable $Li_{1-x-y}H_yCoO_2$ phase is formed [107]. The chemical composition of $Li_{1-x-y}H_yCoO_2$ is specified by a competition between lithium extraction and proton exchange, depending on the acid concentration and on the degree of sample dissolution. These two competitive reactions proceed without destruction of the structural CoO_2 framework of parent $LiCoO_2$.

Proton-exchanged $HCoO_2$ was found to be an efficient anode material for the oxidation of hydrogen in a solid oxide fuel cell [108].

Chemical deintercalation in $LiNi_yCo_{1-y}O_2$

Acid treatment of LT-$LiCoO_2$ and LT-$LiCo_{0.9}Ni_{0.1}O_2$ at room temperature yields delithiated products having the composition $Li_{0.4}CoO_2$ and $Li_{0.4}Co_{0.8}Ni_{0.1}O_2$ [44]. The structure refinement of neutron diffraction data of LT-$Li_{0.4}CoO_2$ gives evidence of a spinel-type structure. It was assumed that LT-$Li_{0.4}Co_{0.8}Ni_{0.1}O_2$ was a defect spinel with spinel notation $\{Li_{0.8}\square_{0.2}\}_{8a}[Co_{1.6}Ni_{0.2}\square_{0.2}]_{16d}O_4$. This spinel phase exhibits better reversibility during lithium insertion/extraction compared to pristine LT-$LiCo_{0.9}Ni_{0.1}O_2$.

New layered materials in the Li-Ni-Co-O system have been obtained by reaction of $(Ni_yCo_{1-y})_3O_4$ ($0 \le y \le 0.2$) and $Ni_yCo_{1-y}O$ ($y \ge 0.8$) with LiOH between 450 °C and 850 °C [49]. As in the case of high-temperature analogues, cobalt substitution for nickel stabilizes the Ni ions and improves the two-dimensionality of the crystal lattice. Chemical deintercalation of the ceramic oxides was carried out by hydrochloric acid treatment. The layered structure is preserved and the average oxidation state of the metal ions increases significantly in the deintercalated products. For cobalt-rich oxide the ion extraction is accompanied by partial

Li^+/H^+ exchange, especially for LT oxides. When acid treatment of $Li_{1-x}(Ni_yCo_{1-y})_{1+x}O_2$ solid solutions proceeds at 0 °C, the ion exchange reactions are suppressed and, as a result, very crystalline oxides $Li_{0.5}(Ni_y$-$Co_{1-y})_{1+x}O_2$, which do not contain protons, are formed [96]. During acid delithiation the oxidation of Ni^{3+} to Ni^{4+} ions proceeds prior to the oxidation of Co^{3+} to Co^{4+}, as in the case of a non-aqueous electrolyte. Pristine and acid delithiated oxides have been studied as intercalation cathode materials in electrochemical test cells using lithium anodes and with $LiClO_4$ as the electrolyte [49, 99, 100]. The cells using delithiated products showed an initial voltage in the 3.5–4 V range and could be discharged without previous charge. Discharge-charge cycles of lithium cells using acid delithiated oxides as cathode materials show a significant improvement of reversibility compared with the charge-discharge cycles of the corresponding pristine samples. The voltages were higher for Co-rich compositions [99, 100]. XRD analysis and IR spectroscopy show good reversibility of lithium insertion and extraction by both chemical and electrochemical procedures (Fig. 7) [49].

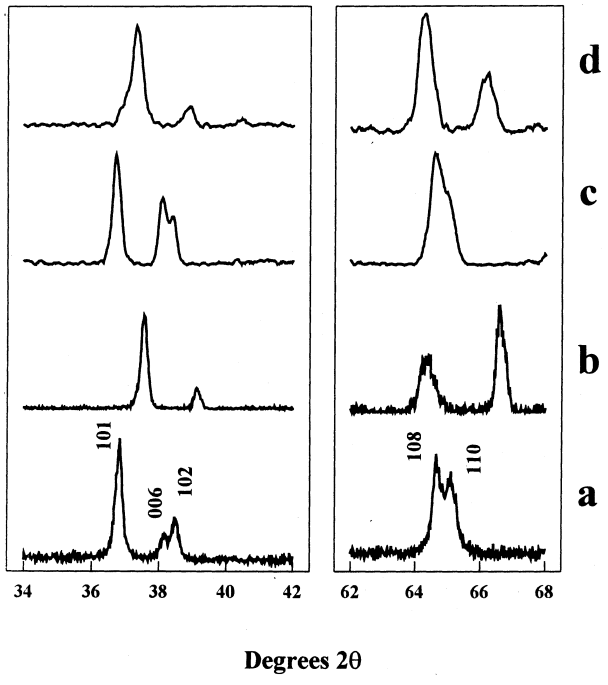

Fig. 7 X-ray powder diffraction data of $Li_{1-x}(Ni_{0.80}Co_{0.20})_{1+x}O_2$ prepared at 850 °C: **a** initial sample, **b** acid-treated sample, **c** after discharge of the cell to 3 V, **d** after cell charge to 4 V

Introduction of other foreign atoms

As was discussed in the previous section, the capacity drop on consecutive charge-discharge cycles is the main operating problem associated with battery performance. An effective way to improve the rechargeability of the cathode material is to make its structure more flexible. Following the materials chemistry rules, the structural modification of solids can be achieved by doping with foreign ions, which may not participate in the redox processes.

Other transition metal atoms

Owing to the structural similarities of the O3 modifications of other lithium transition metal oxides, the synthesis and performance of solids including other atoms different to nickel and cobalt in their composition have been reported. These include:

1. $Li_xMn_yNi_{1-y}O_2$: Rossen et al. [109] reported the synthesis of solid solutions of the $Li_xMn_yNi_{1-y}O_2$ series, which were isostructural with $LiNiO_2$ in the $0 \le y \le 0.6$ range and with $x \approx 1$. In order to obtain single-phase products, it was necessary to use MnO as the source of manganese with $LiOH \cdot H_2O$ and NiO as the starting reagents. The presence of mostly Mn^{3+} was reported in these solid solutions, although the occurrence of Mn^{4+} for $x > 1$ was also suggested. The capacity of lithium cells using these materials as the cathode decreased as y increased [109, 110]. This fact limits the potential applicability of these solids in lithium and lithium-ion cells and was explained by the coupled effects of cation mixing and the presence of Mn^{4+}. Later, Caurant et al. [111, 112] reported an alternative synthesis of the $LiNi_zMn_{1-z}O_2$ series ($0.5 < z < 1$) using a "chimie douce" procedure based on hydroxide: $Ni(OH)_2$ coprecipitation followed by drying and heating at 700 °C. The crystallinity and electrochemical behavior were found to deteriorate with decreasing z, which was interpreted similarly to Rossen et al. [109] as the occurrence of Mn^{4+} ions.

2. $LiFe_yNi_{1-y}O_2$: Rougier et al. [113] communicated the synthesis of layered solids with the $R\bar{3}m$ structure for $LiFe_yNi_{1-y}O_2$ compositions with $0 \le y \le 0.2$. For iron-rich compositions with $y \ge 0.5$ a second solid solution of the cubic α-$LiFeO_2$ type was found, while for intermediate compositions ($0.3 \le y \le 0.5$) these authors found the coexistence of cubic and hexagonal phases. Results of Rietveld refinement were reported, from which a cation distribution of the type $[Li_{0.965}M_{0.035}]_{3b}[M_{0.965}$ $Li_{0.035}]_{3a}O_2$ was obtained for $M = 0.2Fe + 0.8Ni$. Simultaneously, Reimers et al. [114] reported a detailed study of these solids, in which the composition limits were in good agreement with the results of Rougier et al. [113]. Electrochemical measurements carried out in $Li/LiFe$-$_yNi1_{-y}O_2$ showed that the amount of lithium that could be reversibly cycled decreased with y.

3. $LiCr_yCo_{1-y}O_2$: Jones et al. [115] tested the possible formation of $LiCr_yCo_{1-y}O_2$ and $LiCr_yNi_{1-y}O_2$ solid solutions. While attempts to obtain single-phase products were unsuccessful in the nickel case, $Li_xCr_yCo_{1-y}O_2$ products were obtained by heating mixtures of $LiCrO_2$ and $LiCoO_2$ in argon at 950 °C. Rietveld analysis of the solid solutions revealed a smooth evolution of the

crystallographic parameters. Unfortunately, the reversibility of the charging process decreased dramatically with y [115].

p-Block elements

Boron-doped $LiCoO_2$

Several patents have reported that batteries using B-doped $LiCoO_2$ as the active cathode material have improved charge-discharge cycle performance and long life [116, 117].

XRD, ^{6}Li and ^{11}B MAS NMR, IR, and EPR of low-spin Ni^{3+} probes were used for the structural characterization of boron-doped $LiCoO_2$ [118]. Up to 5 at% boron additives were shown to dissolve in trigonal $LiCoO_2$. The structure of the CoO_2 sandwiches remains unaffected by this treatment. The boron environment was assessed by spectroscopic analysis, which show a distorted tetrahedral coordination. The boron-doped $LiCoO_2$ samples were used as active electrode materials in lithium cells. Step potential electrochemical spectroscopy (Fig. 4c) and galvanostatic cycling revealed that boron dopants improve the reversibility of the lithium deintercalation/intercalation process and favor lattice adaptation to lithium order-disorder in the depleted LiO_2 layers.

Aluminum

In principle, the possible replacement of nickel or cobalt by aluminum in the layer of octahedral sites of metal atoms of layered $LiMO_2$ oxides could be expected to be easy, as it exists in one crystalline modification of the mixed lithium aluminum oxide α-$LiAlO_2$, which is isostructural with other O3 $LiMO_2$ compounds.

In order to improve the electrochemical properties of $LiNiO_2$, the formation of $LiNiO_2$-$LiAlO_2$ solid solutions was examined by Zhong and von Sacken [119] and Ohzuku et al. [120, 121]. The synthesis of a single-phase product with $LiAl_yNi_{1-y}O_2$ composition in the complete composition interval was carried out by heating a mixture of $LiNO_3$, $NiCO_3$, and $Al(OH)_3$ at 750 °C under an oxygen stream [120]. The XRD characterization of the solid with $LiAl_{1/4}Ni_{3/4}O_2$ stoichiometry showed that it belongs to the space group $R\bar{3}m$, with $a = 2.86$ Å and $c = 14.24$ Å in hexagonal setting. The behavior of this solid in nonaqueous lithium cells was also examined. $LiAl_{1/4}Ni_{3/4}O_2$ was oxidized to $Li_{1/4}Al_{1/4}Ni_{3/4}O_2$ in the voltage range 3.5–4.8 V. XRD of the charged electrodes obtained with different lithium contents revealed that lithium extraction takes place reversibly by a single-phase mechanism involving the expansion of the layer separation from 4.75 to 4.80 Å. A rechargeable capacity of ca. 150 mAh g^{-1} was reported for this material.

The preparation of solid solutions of the $LiAlO_2$-$LiCoO_2$ system in the complete composition range has also been reported [122]. Powder XRD gives direct information about the partial substitution of Co by Al atoms, together with a fractional occupancy of tetracoordinated sites by aluminum atoms (Fig. 8). EPR of impurity Ni^{3+} ions and ^{6}Li and ^{27}Al MAS NMR spectroscopies were used to assess the cation distribution.The ^{6}Li NMR spectra show a single resonance of lithium ions at octahedral sites. ^{27}Al NMR shows that the distribution of Al atoms in tetrahedral and octahedral sites changes with composition. EPR spectra show that Ni^{3+} impurity ions in the $Al_yCo_{1-y}O_2$ layers prefer mainly Al^{3+} ions as first neighbors. The potential applicability of these materials as intercalation electrodes was also evaluated in lithium anode cells. Poor lithium ion diffusivity, resulting from the presence of aluminum in both tetrahedral and octahedral sites, may limit the applicability of $LiAl_yCo_{1-y}O_2$ cathodes. The partial substitution of Co by Ni leads to an improvement of the electrochemical performance. This effect is particularly evident by comparing the first charge-discharge cycle of the three compositions collected in Fig. 9.

Other layered $LiMO_2$ solids

Layered $LiMnO_2$

Following the search for alternative materials that intercalate lithium ions, the synthesis and electrochemical performance of a new material, layered $LiMnO_2$, was recently reported [123]. The solid was obtained by ion exchange and was found to be structurally analogous to $LiCoO_2$. The charge capacity of lithium cells using layered $LiMnO_2$ as the cathode material was found to be ca. 270 mAh g^{-1}, a value comparable in magnitude to both $LiCoO_2$ and $LiMn_2O_4$. Up to now, however, cycling properties are limited in this solid.

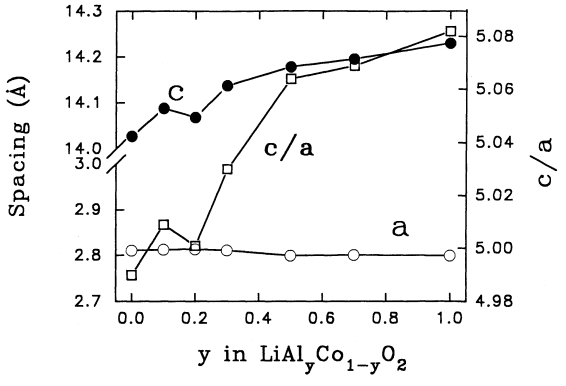

Fig. 8 Changes in the unit cell parameters of $LiAl_yCo_{1-y}O_2$ solid solutions

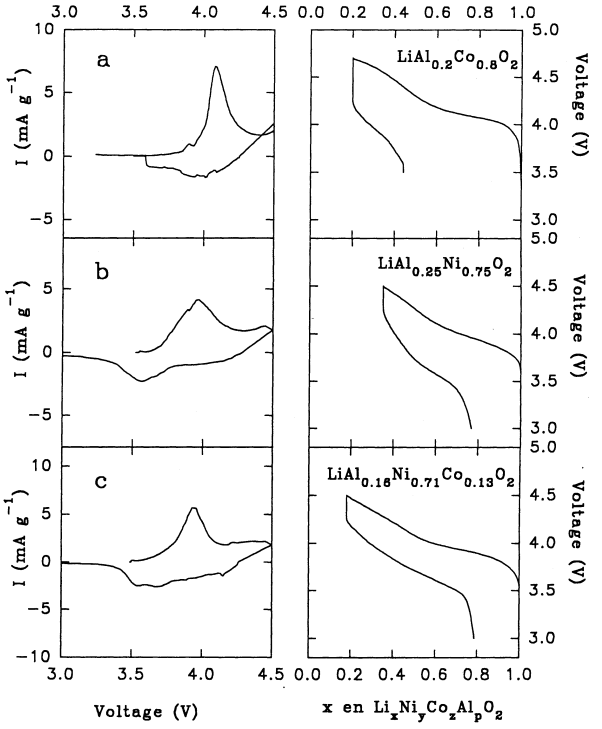

Fig. 9 *Left*: normalized intensity versus voltage. *Right*: voltage versus composition plots obtained by step potential electrochemical spectroscopy of lithium cells using different samples as intercalation electrodes: **a** $LiAl_{0.2}Co_{0.8}O_2$, **b** $LiAl_{0.25}Ni_{0.75}O_2$, **c** $LiAl_{0.16}Ni_{0.71}Co_{0.13}O_2$

Layered $LiFeO_2$

Tabuchi et al. [124–126] reported the synthesis of a metastable form of layered $LiFeO_2$ via a Li^+/Na^+ exchange reaction of α-$NaFeO_2$ performed at 140 °C with a large excess of $LiOH \cdot H_2O$, either in methanol or in ethanol. Alternatively, this material can be obtained directly from α-FeOOH or $FeCl_3 \cdot 6\,H_2O$ by hydrothermal reaction at 230 °C using aqueous mixed-alkaline solutions such as $LiOH \cdot H_2O$-KOH or $LiOH \cdot H_2O$-NaOH. The XRD data of the highly crystallized products obtained from both the hydrothermal and ion-exchanged sample are indexable using the rhombohedral (hexagonal) unit cell of layered $LiFeO_2$. However, preliminary tests on electrochemical lithium deintercalation/intercalation show poor performance between 4.5 and 1.5 V.

Layered $LiCrO_2$. Solid solutions with $LiAlO_2$

Layered $LiCrO_2$ is isostructural with $LiCoO_2$ (O3), but displays poor capability for lithium extraction in the potential range 3.6–4.0 V [127, 128]. As a compensation, the proton exchange reactions are facilitated for $LiCrO_2$. The hydrothermal treatment of $LiCrO_2$ leads to its conversion into the isostructural oxyhydroxide α-$HCrO_2$ [129]. The reaction takes place without changes in particle size and shape owing to its topotactic nature.

The solid solution $LiAl_xCr_{1-x}O_2$ was first synthesized by Poeppelmeier and Thong [130] over the complete range $0 < x < 1$ by using boehmite as the alumina source. The linear variation of the unit cell parameters with the aluminum composition of the solid solution was in agreement with Vegard's law. For $x > 0.6$, the α-$LiAlO_2$ structure containing chromium in octahedral sites was stabilized. Cation replacement of Li^+ with H^+ in both α-$LiAlO_2$ and α-$LiAl_xCr_{1-x}O_2$ has also been reported [131].

Acknowledgement The authors acknowledge financial support of CE, contract JOU2-CT93-0326 and supplementary agreement CIPD-CT94-0501.

References

1. Ohzuku T (1994) Lithium batteries. New materials, developments and perspectives. In: Pistoia G (ed) Elsevier, Amsterdam, p 239
2. Salomon M, Scrosati B (1996) Gazz Chim Ital 126: 415
3. Owen JK (1997) Chem Soc Rev 26: 259
4. Idota Y, Kubota T, Matsufuji A, Maekawa Y, Miyasaka T (1997) Science 276: 1395
5. Rahner D, Machill S, Schlörb H, Siury K, Kloss M, Plieth W (1998) J Solid State Electrochem 2: 78
6. Koksbang R, Barker J, Shi H, Sa MY (1996) Solid State Ionics 84: 1
7. Bruce PG (1997) J Chem Soc Chem Commun 1817
8. Nagaura T, Tazawa K (1990) Prog Batteries Col Cells 9: 20
9. Dyer LD, Borie BS, Smith GP (1954) J Am Chem Soc 76: 1499
10. Goodenough JB, Wickham DG, Croft WJ (1958) J Phys Chem Solids 5: 107
11. Bronger VW, Bade H, Klemm W (1964) Z Anorg Allg Chem 333: 188
12. Morales J, Pérez-Vicente C, Tirado JL (1990) Mater Res Bull 25: 623
13. Pickering IJ, Maddox PJ, Thomas JM (1992) Chem Mater 4: 994
14. Dahn JR, von Sacken U, Michal CA (1990) Solid State Ionics 44: 87
15. Li W, Reimers JN, Dahn JR (1992) Phys Rev B 46: 3236
16. Rougier A, Gravereau P, Delmas C (1996) J Electrochem Soc 143: 1168
17. Alcantara R, Lavela P, Tirado JL, Stoyanova R, Kuzmanova E, Zhecheva E (1997) Chem Mater 9: 2145
18. Pickering IJ, George GN, Lewandowski JT, Jacobson AJ (1993) J Am Chem Soc 115: 4137
19. Atanasov M, Reinen D (1997) J Electron Specrosc Relat Phenom 86: 185
20. Stoyanova R, Zhecheva E, Friebel C (1993) J Phys Chem Solids 54: 9
21. Azzoni CB, Paleari A, Massarotti V, Bini M, Capsoni D (1996) Phys Rev B 53: 703
22. van Elp J, Eskes H, Kuiper P, Sawatzky GA (1992) Phys Rev B 45: 1612
23. Mackrodt WC, Harrison NM, Saunders VR, Alan NL, Towler MD (1996) Chem Phys Lett 250: 66
24. Kemp JP, Cox PA, Hodby JW (1990) J Phys Condens Matter 2: 6699
25. Duta G, Manthiram, Goodenough JP, Grenier JC (1992) J Solid State Chem 96: 123
26. Reimers JN, Dahn JR, Greedan JE, Stager CV, Liu G, Davidson I, von Sacken U (1993) J Solid State Chem 102: 542
27. Rougier A, Delmas C, Chadwick AV (1995) Solid State Commun 94: 123

28. Rougier A, Chadwick AV, Delmas C (1995) Nucl Inst Methods Phys Res B 97: 75
29. Ohzuku T, Ueda A, Nagayama M (1993) J Electrochem Soc 140: 1862
30. Li W, Reimers JN, Dahn JR (1993) Solid State Ionics 67: 123
31. Broussely M, Perton F, Labat J, Staniewicz RJ, Romero A (1993) J Power Sources 43–44: 209
32. Broussely M, Perton F, Biensan P, Bodet JM, Labat J, Lecerf A, Delmas C, Rougier A, Peres JP (1995) J Power Sources 54: 109
33. Dahn JR, von Sacken U, Juskow MW, Al-Janabi J (1991) J Electrochem Soc 138: 2207
34. Arai H, Okada S, Ohtsuka H, Ichimura M, Yamaki J (1995) Solid State Ionics 80: 261
35. Kanno R, Kubo H, Kawamoto Y, Kamiyama T, Izumi F, Takeda YY, Takano M (1993) J Solid State Chem 102: 543
36. Moshtev RV, Zlatilova P, Manev V, Sato A (1995) J Power Sources 54: 329
37. Delmas C, Pérès JP, Rougier A, Demourgues A, Weill F, Chadwick A, Broussely M, Perton F, Biensan P, Willmann P (1997) J Power Sources 68: 120
38. Choi YM, Pyun SI, Bal JS, Moon SI (1995) J Power Sources 56: 25
39. Johnston WD, Heikes RR, Sestrich D (1958) J Phys Chem Solids 7: 1
40. Orman HJ, Wiseman PJ (1984) Acta Crystallogr C 40: 12
41. van Elp J, Wieland JL, Eskes H, Kuiper P, Sawatzky GA (1991) Phys Rev B 44: 6090
42. Galakhov VR, Kurmaev EZ, Uhlenbrock St, Neuman M, Kellrman DG, Gorshkov VS (1996) Solid State Commun 99: 221
43. Gummow RJ, Thackeray MM (1992) Solid State Ionics 53–56: 681
44. Gummow RJ, Thackeray MM (1993) J Electrochem Soc 140: 3365
45. Gummow RJ, Thackeray MM, David WIF, Hull S (1992) Mater Res Bull 27: 327
46. Gummow RJ, Liles DC, Thackeray MM (1993) Mater Res Bull 28: 235
47. Gummow RJ, Liles DC, Thackeray MM, David WIF (1993) Mater Res Bull 28: 1177
48. Rossen E, Reimers JN, Dahn JR (1993) Solid State Ionics 62: 53
49. Morales J, Stoyanova R, Tirado JL, Zhecheva E (1994) J Solid State Chem 113: 182
50. Garcia B, Barboux P, Ribot F, Kahn-Harari A, Mazerolles L, Baffier N (1995) Solid State Ionics 80: 111
51. Huang WW, Frech R (1996) Solid State Ionics 86–88: 395
52. Carewska M, Scaccia S, Croce F, Arumugam S, Wang Y, Greenbaum S (1997) Solid State Ionics 93: 227
53. Reimers JN, Dahn JR (1992) J Electrochem Soc 139: 2091
54. Ohzuku T, Ueda A (1994) J Electrochem Soc 141: 2972
55. Amatucci GG, Tarascon JM, Klein LC (1996) J Electrochem Soc 143: 1114
56. Mizushima K, Jones PC, Wiseman PJ, Goodenough JB (1980) Mater Res Bull 15: 783
57. Amatucci GG, Tarascon JM, Klein LC (1996) Solid State Ionics 83: 167
58. Ohzuku T, Ueda A, Nagayama M, Iwakoshi Y, Komori H (1993) Electrochim Acta 38: 1159
59. Barker J, Pynenburg R, Koksbang R, Saïdi MY (1996) Electrochim Acta 41: 2481
60. Honders A, der Kinderen JM, van Heeren AH, Wit JHW, Broers GHJ (1985) Solid State Ionics 15: 265
61. Garcia B, Farcy J, Pereira-Ramos JP, Perichon J, Baffier N (1995) J Power Sources 54: 373
62. Garcia B, Farcy J, Pereira-Ramos JP, Baffier N (1997) J Electrochem Soc 144: 1179
63. Ouyang B, Chao X, Lin HW, Slane S, Kostov S, den Boer M, Greenbaum SG (1995) Mater Res Soc Symp Proc 369: 59
64. Ohzuku T, Komori H, Swai K, Hirai T (1990) Chem Express 5: 733
65. Delmas C, Saadoune I (1992) Solid State Ionics 53–56: 370
66. Delmas C, Saadoune I, Rougier A (1993) J Power Sources 44: 595
67. Rougier A, Saadoune I, Gravereau P, Willmann P, Delmas C (1996) Solid State Ionics 90: 83
68. Zhecheva E, Stoyanova R (1993) Solid State Ionics 66: 143
69. Ohzuku T, Ueda A, Masatoshi N, Yasunobu I, Komori H (1993) Electrochim Acta 38: 1159
70. Ueda A, Ohzuku T (1994) J Electrochem Soc 141: 2010
71. Menetrier M, Rougier A, Delmas C (1994) Solid State Commun 90: 439
72. Marichal C, Hirschinger J, Granger P, Menetrier M, Rougier A, Delmas C (1995) Inorg Chem 34: 1773
73. Stoyanova R, Zhecheva E, Alcántara R, Lavela P, Tirado JL (1997) Solid State Commun 102: 457
74. Saadoune I, Delmas C (1996) J Mater Chem 6: 193
75. Alcántara R, Lavela P, Tirado JL, Zhecheva E, Stoyanova R (1998) J Electrochem Soc 145: 730
76. Dunn B, Farrington GC, Katz B (1994) Solid State Ionics 70–71: 3
77. Schleich DM (1994) Solid State Ionics 70–71: 407
78. Pereira-Ramos JP (1995) J Power Sources 54: 120
79. Barboux P, Tarascon JM, Shokoohi FK (1991) J Solid State Chem. 94: 185
80. Sun YK, Oh IH, Hong SA (1996) J Mater Sci 31: 3617
81. Sun YK, Oh IH (1997) J Mater Sci Lett 16: 30
82. Barriga C, Calero A, Morales J, Tirado JL (1989) React Solids 7: 263
83. Yoshio M, Tanaka H, Tominaga K, Noguchi H (1992) J Power Sources 40: 347
84. Yazami R, Lebrun N, Bonneau M, Molteni M (1995) J Power Sources 54: 389
85. Chen CH, Buysman AAJ, Kelder EM, Schoonman J (1995) Solid State Ionics 80: 1
86. Fragnaud P, Nagarajan R, Schleich DM, Vujic D (1995) J Power Sources 54: 362
87. Antaya M, Cearns K, Preston JS, Reimers JN, Dahn JR (1994) J Appl Phys 76: 2799
88. Antaya M, Dahn JR, Preston JS, Rossen E, Reimers JN (1993) J Electrochem Soc 140: 575
89. Striebel KA, Deng CZ, Wen SJ, Cairns EJ (1996) J Electrochem Soc 143: 1821
90. Fragnaud P, Schleich DM (1995) Sensors Actuators A51: 21
91. Fragnaud P, Schleich DM (1995) Ionics 1: 183
92. Brousse T, Fragnaud P, Marchand R, Schleich DM (1996) Ionics 2: 398
93. Chang HSW, Lee TJ, Lin SC, Jeng JH (1995) J Power Sources 54: 403
94. Zhecheva E, Stoyanova R, Gorova M, Alcántara R, Morales J, Tirado JL (1996) Chem Mater 8: 1429
95. Zhecheva E, Stoyanova R, Gorova M, Alcantara R, Morales J, Tirado JL (1997) Ionics 3: 1
96. Amatucci GG, Tarascon JM, Larcher D, Klein LC (1996) Solid State Ionics 84: 169
97. Larcher D, Palacin MR, Amatucci GG, Tarascon JM (1997) J Electrochem Soc 144: 408
98. Palacin MR, Larcher D, Audemer A, Sac-Epee N, Amatucci GG, Tarascon JM (1997) J Electrochem Soc 144: 4226
99. Alcántara R, Morales J, Tirado JL, Stoyanova R, Zhecheva E (1995) J Electrochem Soc 142: 3997
100. Alcántara R, Morales J, Stoyanova R, Tirado JL, Zhecheva E (1995) Ionics 1: 246
101. Stoyanova R, Zhecheva E (1994) J Solid State Chem 108: 211
102. Morales J, Pérez–Vicente C, Tirado JL (1992) J Thermal Anal 38: 295
103. Dahn JR, Fuller EW, Obrovac M, von Sacken U (1994) Solid State Ionics 69: 265
104. Fernández JM, Hernán L, Morales J, Tirado JL (1988) Mater Res Bull 23: 899
105. Delaplane RG, Ibers JA (1969) J Chem Phys 50: 1920
106. Fernández JM, Morales J, Tirado JL (1987) React Solids 4: 163

107. Zhecheva E, Stoyanova R (1994) J Solid State Chem 109: 47
108. Sato K, Hagizaka S, Inoue Y (1993) Solid State Ionics 66: 197
109. Rossen E, Jones CWD, Dahn JR (1992) Solid State Ionics 57: 311
110. Nitta Y, Okamura K, Haraguchi K, Kobayaschi S, Ohta A (1995) J Power Sources 54: 511
111. Caurant D, Baffier N, Bianchi V, Grégoire G, Bach S (1996) J Mater Chem 6: 1149
112. Caurant D, Baffier N, Garcia B, Pereira-Ramos JP (1996) Solid State Ionics 91: 45
113. Rougier A, Gravereau P, Delmas C, Willmann P (1993) GFECI (Groupe Francais d'Etude des Composes d'Insertion, 1993, Clermont-Ferrant, France)
114. Reimers JN, Rossen E, Jones CD, Dahn JR (1993) Solid State Ionics 61: 335
115. Jones CDW, Rossen E, Dahn JR (1994) Solid State Ionics 68: 65
116. Toyoguchi Y (1990) Eur Pat Appl 90106149.9
117. Mizutani M, Fukunaga T (1993) Jpn Kokai Tokyo Koho JP 05,325,971; Mizutani M, Fukunaga T (1992) JP Appl 92/47,942
118. Alcántara R, Lavela P, Tirado JL, Zhecheva E, Stoyanova R (1997) J Solid State Chem 134: 265
119. Zhong Q, von Sacken U (1995) J Power Sources 54: 221
120. Ohzuku T, Ueda A, Kouguchi M (1995) J Electrochem Soc 142: 4033
121. Ohzuku T, Yanagawa T, Kouguchi M, Ueda A (1997) J Power Sources 68: 131
122. Alcantara R, Lavela P, Relaño PL, Tirado JL, Zhecheva E, Stoyanova R (1998) Inorg Chem 37: 264
123. Armstrong AR, Bruce PG (1996) Nature 381: 499
124. Tabuchi M, Ado K, Sakaebe H, Masquelier C, Kageyama H, Nakamura O (1995) Solid State Ionics 79: 220
125. Tabuchi M, Masquelier C, Takeuchi T, Ado K, Matsubara I, Shirane T, Kanno R, Tsutsui S, Nasu S, Sakaebe H, Nakamura O (1996) Solid State Ionics 90: 129
126. Ado K, Tabuchi M, Kobayashi H, Kageyama H, Nakamura O, Inaba Y, Kanno R, Takagi M, Takeda Y (1997) J Electrochem Soc 144: L177
127. Miyazaki S, Kikkawa S, Koizumi M (1983) Synth Met 6: 211
128. Kikkawa S, Miyazaki S, Koizumi M (1985) J Power Sources 14: 231
129. Hernán L, Macías M, Morales J, PérezVicente C, Tirado JL (1989) Mater Res Bull 24: 781
130. Poeppelmeier KR, Thong SH (1989) J Less Common Metals 156: 291
131. Poeppelmeier KR, Kipp DO (1988) Inorg Chem 27: 66